Food Chemistry 305 (2020) 125482

Contents lists available at ScienceDirect

Food Chemistry

journal homepage: www.elsevier.com/locate/foodchem

Characterization of initial reaction intermediates in heated model systems of glucose, glutathione, and aliphatic aldehydes

Tianze Wang[a], Dawei Zhen[b], Jia Tan[a], Jianchun Xie[a,*], Jie Cheng[c], Jian Zhao[a]

[a] Beijing Advanced Innovation Center for Food Nutrition and Human Health, Beijing Technology and Business University (BTBU), Beijing 100048, China
[b] Beijing Lanjingzhongyu Scientific Development Co. Ltd, Beijing 100048, China
[c] Institute of Quality Standard and Testing Technology for Agro-products of CAAS, Beijing 100081, China

ARTICLE INFO

Keywords:
Glutathione
Aliphatic aldehyde
Intermediate
Mechanism
Meat flavor
Maillard reaction
Lipid degradation

ABSTRACT

To understand the effect of lipid degradation on Maillard formation of meaty flavors, initial reaction intermediates in model systems of glucose–glutathione with hexanal, (*E*)-2-heptenal, or (*E*,*E*)-2,4-decadienal were identified by HPLC–MS and by NMR. Besides Amadori compounds, hemiacetals and thiazolidines via addition of sulfhydryl to carbonyl or to the conjugated olefinic bond were found. Concentrations of all intermediates increased with reaction time while degradation of the intermediates with a glutathione moiety helped formation of thiazolidines with cysteinylglycine. The unsaturated aldehydes (*E*)-2-heptenal and (*E*,*E*)-2,4-decadienal exhibited high reactivity against glucose for glutathione, yielding higher levels of intermediate compounds than from glucose. Heating prepared intermediates reversibly released the original aldehydes, which caused various compounds formed by retro-aldol, oxidation, etc. to react with H_2S and NH_3. Among them, formation pathways including 3-nonen-2-one, 2-hexanoylfuran, and six dialkylthiophenes (e.g., 2-ethyl-5-(1-methylbutyl)thiophene) were proposed for the first time.

1. Introduction

Glutathione (γ-Glu-Cys-Gly, GSH), which exists in most living animals and plants, functions in protecting cells from toxins such as free radicals and peroxides, due to its reducing and nucleophilic properties (Pan et al., 2014; Schumacher et al., 2017). In food systems, similar to cysteine, GSH is known as an important meaty flavor precursor, which can release H_2S from cysteine and result in formation of various sulfur-containing meaty flavors (El-massry, Farouk, & El-Ghorab, 2003; Lee, Jo, & Kim, 2010; Zhou, Grant, Goldberg, Ryland, & Aliani, 2018). Previous findings demonstrated that lipid degradation affected the Maillard reaction of cysteine and reducing sugars to produce meaty flavor compounds (Elmore, Campo, Enser, & Mottram, 2002; Farmer & Mottram, 1990; Yang et al., 2015). With the inclusion of a lipid, the amount of sulfur-containing flavors formed was decreased, while some new alkyl sulfur compounds (e.g., 2-hexylthiophene) were generated. A recent investigation (Zhao, Wang, Xie, Xiao, Cheng, et al., 2019) revealed similar effect of lipids upon the Maillard reaction of GSH and glucose in the production of sulfur-containing meaty flavors. Nevertheless, it remains unclear how lipids affect the Maillard reaction to form meaty flavors.

When lipids are included in the Maillard reaction of reducing sugars and amino compounds such as GSH, initially, reducing sugars will react with the amino compounds to form non-volatile intermediates, especially the Amadori rearrangement compounds, which are critical for development of volatile flavor compounds (Hou et al., 2017; Liu, Zhang, Huang, Song, & Nsor-Atindana, 2012). On the other hand, the lipid degradation products of carbonyl compounds also react with the amino compounds, forming non-volatile intermediates that can play roles in the development of volatile food flavors (Starkenmann, 2003). For example, it was reported that 3-*S*-glutathionylhexanal from reaction of (*E*)-2-hexenal and GSH was the precursor of 3-mercapto-1-hexanol in grape juices (Clark & Deed, 2018; Thibon et al., 2016). Therefore, in this study, from the point of formation of non-volatile initial intermediates, reaction model systems of GSH and glucose with hexanal, (*E*)-2-heptenal, or (*E*,*E*)-2,4-decadienal, the typical carbonyls from fat oxidation and degradation (Yang et al., 2015; Zhao, Wang, Xie, Xiao, Cheng, et al., 2019), were investigated. Structures of the found initial intermediate compounds in reaction mixtures were characterized by HPLC–MS and NMR, and the roles of the aldehyde-derived intermediates in development of volatile flavors were exposed by thermal degradation of the prepared intermediates. The object of the work is to gain insight into the flavor formation mechanism involving Maillard reaction with the lipid degradation during processing of meat or meat-like foods.

* Corresponding author.
E-mail address: xjchun@th.btbu.edu.cn (J. Xie).

https://doi.org/10.1016/j.foodchem.2019.125482
Received 16 March 2019; Received in revised form 4 September 2019; Accepted 4 September 2019
Available online 05 September 2019

2. Experimental

2.1. Materials and chemicals

L-Glutathione (99%), D-glucose (98%), hexanal (95%), (*E*)-2-heptenal (95%), (*E*,*E*)-2,4-decadienal (93%), and the authentic chemicals (≥95%) for identification of volatile flavors were purchased from J&K Chemical Ltd. (Beijing, China). The *n*-alkanes (C_5–C_{26}) for determination of retention indices and other chemicals used were all of analytical grade and purchased from Sinopharm Chemical Reagent Co., Ltd. (Beijing, China).

2.2. Model reactions

Three model reaction systems, i.e., glucose, glutathione, and hexanal (Glu-GSH-Hex); glucose, glutathione, and (*E*)-2-heptenal (Glu-GSH-Hept); and glucose, glutathione, and (*E*,*E*)-2,4-decadienal (Glu-GSH-Dec); along with the control systems, i.e., glutathione and glucose (GSH-Glu); glutathione and hexanal (GSH-Hex); glutathione and (*E*)-2-heptenal (GSH-Hept); and glutathione and (*E*,*E*)-2,4-decadienal (GSH-Dec), were performed.

The amounts of reactants used were GSH (0.30 mmol), glucose (0.30 mmol), and aldehyde (0.70 mmol, each). The reactants were weighed according to the respective systems and dissolved in 5 mL of phosphate buffer (0.2 M, pH 6.5) in a 15-mL pressure resistant tube. Then the tubes were sealed and heated at 140 °C while stirring for 0.16, 0.25, 0.5, 1, 2, 3, or 4 h. Two replicates were performed. The reaction mixtures were subjected to HPLC–MS analysis, as described in Section 2.5.

2.3. Preparation of the intermediate compounds (L1, M2, M3, N4, and N5)

2.3.1. L1

GSH (0.184 g, 0.6 mmol) and hexanal (0.060 g, 0.6 mmol) were first dissolved in 5 mL of phosphate buffer (0.2 M, pH 6.5) in a 15-mL pressure-resistant tube, and then heated at 90 °C for 80 min. The obtained reaction mixture was separated on a column (1.6 cm × 40 cm) packed with AG 50W-X4 cation exchange resin (63–150 μm) (Bio-Rad Co., Ltd., Shanghai, China) by a MD-99 automatic liquid chromatographic system (Shanghai Qingpu Huxi Instruments Co., Shanghai, China) with UV monitoring at 220 nm. The reaction mixture was entirely loaded on the column. The column was first washed with 100 mL of water, and then eluted gradually with 200 mL of ammonium hydroxide (0.3 M). The target fractions were collected and freeze dried, yielding 0.1 g of product L1. The product L1 was subjected to HPLC–ELSD, HPLC–MS, and ^{1}H NMR and ^{13}C NMR analyses. Regarding the NMR analysis, an AV 600 NMR spectrometer (Bruker, Switzerland) was used with D_2O as the solvent and tetramethylsilane as the internal standard.

Purity of the product L1 was 99% according to relative peak area by HPLC–ELSD analysis. HPLC-(ESI^+) MS: 261($[M+H]^+$). ^{1}H NMR (600 MHz, D_2O, ppm): δ 0.78 (t, J = 6.4 Hz, CH_3-11), 1.20–1.43 (m, CH_2-8, CH_2-9, CH_2-10), 1.66–1.86 (m, CH_2-7), 3.05–3.24 (m, CH_2-5), 3.67–3.80 (m, CH_2-2, CH-4), 4.61–4.65 (m, CH-6). ^{13}C NMR (150 MHz, D_2O, ppm): δ 13.20 (C-11), 21.75 (C-10), 25.56 (C-8), 30.76 (C-9), 35.37 (C-5), 37.58 (C-7), 43.20 (C-2), 64.91 (C-6), 69.84 (C-4), 172.01, 176.45 (C-1, C-3), 184.36 (C-1, COO^-).

2.3.2. M2

GSH (0.276 g, 0.9 mmol) and (*E*)-2-heptenal (0.067 g, 0.6 mmol) were first dissolved in 5 mL of phosphate buffer (0.2 M, pH 6.5) in a 15-mL pressure-resistant tube, and then heated at 90 °C for 10 min. The resulting reaction mixture was separated on a column (1.6 cm × 40 cm) packed with HP 20SS macroporous resin (Mitsubishi Chemical Corporation, Tokyo, Japan) using the above automatic liquid chromatographic system with UV monitoring at 220 nm. The entire reaction mixture was loaded on the column. The column was eluted gradually with 200 mL of 40% ethanol. The target fractions were collected and freeze-dried, yielding 0.1 g of product M2. Similarly, the product M2 was subjected to HPLC–ELSD, HPLC–MS, and ^{1}H NMR and ^{13}C NMR analyses.

Purity of the product M2 was 99% according to relative peak area by HPLC–ELSD analysis. HPLC-(ESI^+) MS: 420 ($[M+H]^+$). ^{1}H NMR (600 MHz, D_2O, ppm): δ 0.75–0.82 (m, CH_3-17), 1.15–1.36 (m, CH_2-15, CH_2-16), 2.01–2.13 (m, CH_2-3, CH_2-4, CH_2-14), 2.84–2.91 (m, CH_2-10), 3.75 (t, J = 6.30 Hz, CH-2), 3.90 (s, CH_2-8), 4.45–4.54 (m, CH-6), 4.99–5.11 (m, CH-11), 8.35–8.47 (NH-CO); others: Others: 1.45–1.60 (m, CH_2-14′), 2.95–3.08 (m, CH_2-10′), 3.12–3.24 (m, CH_2-11′). ^{13}C NMR (150 MHz, D_2O, ppm): δ 13.21 (C-17), 21.80 (C-16), 25.31 (C-3), 25.92 (C-15), 31.11 (C-10), 31.23 (C-4), 34.12 (C-14), 41.42 (C-8), 53.68 (C-2), 55.57 (C-6), 89.26 (C-11), 125.82 (C-12), 129.14 (C-13), 172.41–175.10 (C-1, C-5, C-7, C-9), 177.61, 181.86 (C-1 or C-9 for COO^-); others: 24.66 (C-14′), 28.11 (C-10′), 38.59 (C-11′), 39.51 (C-13′), 57.52 (C-6′), 206.38 (C-12′).

2.3.3. M3

GSH (0.460 g, 1.5 mmol) and (*E*)-2-heptenal (0.067 g, 0.6 mmol) were first dissolved in 5 mL of phosphate buffer (0.2 M, pH 6.5) in a 15-mL pressure-resistant tube, and then heated at 90 °C for 80 min. The resulted reaction mixture was separated on a column (3.0 cm × 60 cm) packed with polyamide resin (125–150 μm) (Mitsubishi Chemical Corporation, Tokyo, Japan) using the above automatic liquid chromatographic system with UV monitoring at 220 nm. The reaction mixture was entirely loaded the column. The column was first washed with 300 mL of water, and then eluted gradually with 500 mL of ammonium hydroxide (0.3 M). The target fractions were collected and freeze-dried, yielding 0.06 g of product M3. Similarly, the product M3 was subjected to HPLC–ELSD, HPLC–MS, and ^{1}H NMR and ^{13}C NMR analyses.

Purity of the product M3 was 94% in relative peak area by HPLC–ELSD analysis. HPLC-(ESI^+) MS: 580 ($[M+H]^+$). ^{1}H NMR (600 MHz, D_2O, ppm): δ 0.75 (t, J = 6.6 Hz, CH_3-4′), 1.10–1.33 (m, CH_2-2′, CH_2-3′), 1.38–1.58 (m, CH_2-1′), 1.94–2.10 (m, CH_2-3, CH_2-4, CH_2-12), 2.60–2.66 (m, CH-11), 2.68–3.07 (m, CH_2-10), 3.10–3.34 (m, CH_2-14), 3.59–3.75 (m, CH-2, CH_2-8, CH-15, CH_2-17), 4.39–4.48 (m, CH-6), 4.73–4.80 (m, CH-13). ^{13}C NMR (150 MHz, D_2O, ppm): δ 13.35 (C-4′), 21.76 (C-3′), 26.08 (C-3), 27.96 (C-2′), 30.51 (C-4), 31.38 (C-1′), 33.36 (C-10), 34.80 (C-14), 38.68 (C-12), 42.98 (C-8), 43.43 (C-17), 44.45 (C-11), 52.52 (C-2), 57.37 (C-6), 64.75 (C-13), 66.29 (C-15), 171.66–176.28 (C-1, C-5, C-7, C-9, C-16, C-18).

2.3.4. N4 and N5

GSH (0.460 g, 1.5 mmol) and (*E*,*E*)-2,4-decadienal (0.228 g, 1.5 mmol) were first dissolved in 5 mL of phosphate buffer (0.2 M, pH 6.5) in a 15-mL pressure-resistant tube, and then heated at 90 °C for 5 min. The resulted reaction mixture was separated on a column (3.0 cm × 60 cm) packed with polyamide resin (125–150 μm) (Mitsubishi Chemical Corporation, Tokyo, Japan) using the above automatic liquid chromatographic system with UV monitoring at 220 nm. The reaction mixture was entirely loaded on the column. The column was first washed with 300 mL of water, and then eluted gradually with 500 mL of ammonium hydroxide (0.3 M). The target fractions were freeze-dried and collected, yielding 0.02 g of product N4 and 0.08 g of product N5, respectively. Similarly, the products N4 and N5 were subjected to HPLC–ELSD, HPLC–MS, and ^{1}H NMR and ^{13}C NMR analyses.

N4 and N5 both had a purity of 94% in relative peak area by HPLC–ELSD analysis. Regarding N4, HPLC-(ESI^+) MS: 460 ($[M+H]^+$). ^{1}H NMR (600 MHz, D_2O, ppm): δ 0.70–0.82 (m, CH_3-20), 1.12–1.37 (m, CH_2-17, CH_2-18, CH_2-19), 1.94–2.20 (m, CH_2-3, CH_2-4, CH_2-16), 2.74–2.97 (m, CH_2-10), 3.54–3.80 (m, CH-2, CH_2-8), 4.42–4.55 (m, CH-6), 5.13–5.23 (m, CH-11), 5.28–5.40 (m, CH-15), 5.48–5.56 (m, CH-12), 5.57–5.67 (m, CH-14), 6.13–6.21 (m, CH-13), 7.29, 8.36 (NH-CO);

others: 1.42–1.55 (m, CH_2-15′), 3.08–3.29 (m, CH_2-10′, CH_2-10″), 4.20–4.28 (m, CH-6′), 6.76–6.89 (m, CH-13′). ^{13}C NMR (150 MHz, D_2O, ppm): δ 13.34 (C-20), 21.83 (C-19), 25.45 (C-3), 26.09 (C-17), 30.54 (C-4), 31.37 (C-18), 37.22 (C-10), 38.69 (C-16), 43.25 (C-8), 54.05 (C-2), 55.60 (C-6), 78.96 (C-11), 128.59 (C-14), 128.63 (C-13), 128.75 (C-12), 133.98 (C-15), 171.65–176.24 (C-1, C-5, C-7, C-9); others: 25.30 (C-13″), 28.00 (C-15′), 33.36 (C-10′), 35.40 (C-14′), 58.30 (C-6′), 64.68 (C-6″), 81.82 (C-12″), 122.34 (C-12′), 149.08 (C-13′).

Regarding N5, HPLC-(ESI$^+$) MS: 620 ($[M+H]^+$). ^{1}H NMR (600 MHz, D_2O, ppm): 0.68–0.78 (m, CH_3-7′), 1.07–1.33 (m, CH_2-4′, CH_2-5′, CH_2-6′), 1.90–2.13 (m, CH_2-3, CH_2-3′, CH_2-4, CH_2-12), 2.68–2.90 (m, CH_2-10), 2.92–3.12 (m, CH_2-14), 3.14–3.25 (m, CH-11), 3.49–3.80 (m, CH-2, CH_2-8, CH-15, CH_2-17), 4.35–4.56 (m, CH-6), 5.06–5.16 (m, CH-13), 5.44–5.49 (m, CH-2′), 5.52–5.62 (m, CH-1′), 6.11–8.31 (NH-CO). ^{13}C NMR (150 MHz, D_2O, ppm): δ 13.31 (C-7′), 21.90 (C-6′), 26.32 (C-3), 28.05 (C-4′), 30.38 (C-4), 31.40 (C-5′), 35.34 (C-10), 36.42 (C-3′), 38.55 (C-14), 39.77 (C-12), 43.19 (C-8), 43.33 (C-17), 52.48 (C-11), 53.20 (C-2), 54.06 (C-6), 65.22 (C-13), 67.55 (C-15), 128.81 (C-1′), 135.67 (C-2′), 171.77–176.30 (C-1, C-5, C-7, C-9, C-16, C-18).

2.4. HPLC–ELSD analysis

An Agilent 1260 HPLC system coupled with a 1260 Infinity evaporative light scattering detector (ELSD) (Agilent Technologies, Santa Clara, CA) was used. The temperature of the ELSD evaporation tube was 40 °C. The flow rate of nitrogen (99.99%) for the evaporation tube was 3.5 mL/min. Chromatographic separation was performed by an Xbridge Amide column (4.6 mm × 150 mm, 3.5 μm; Waters Co., Milford, MA). Mobile phase was composed of acetonitrile and ammonium formate (10 mM; 75:25, v/v), flowing in isocratic elution mode at 1 mL/min. Column temperature was kept at 40 °C. The injection volume of sample was 1 μL.

2.5. HPLC–MS analysis

An LCQ-DECA XP MAX LC–MS system equipped with HPLC and trap tandem mass spectrometer (Thermo-Electron Company, San Jose, CA) was used. HPLC conditions used were identical to those described in the above HPLC–ELSD analysis. Electrospray ionization (ESI) was operated in a positive mode. Ion source voltage was 4.5 kV. Ion source current was 80 μA. Capillary temperature was 350 °C. Flow rates of the sheath gas and auxiliary gas were 60 arb and 20 arb, respectively. Full scan range of mass spectra was set over m/z 50–2000 while for MS/MS detection the collision energy was set at 24%. Data were acquired with Xcalibur software system.

Concentrations of the intermediate compounds in reaction mixtures of the Glu-GSH-Hex, Glu-GSH-Hept, and Glu-GSH-Dec systems were determined as follows. Selected ion monitoring (SIM) mode by monitoring the respective $[M+H]^+$ ion was adopted in MS detection, while GSH was used as the internal standard. First, HPLC–MS analyzed samples of 0.16-h reaction mixtures from the three model systems that were 0, 4, 10, 20, 30, and 100-folds diluted with distilled water, in order to get response factors (ρ) of the found intermediates *vs* GSH. The ρ was calculated by k_i / k_0, where k_i and k_0 were slopes measured by correlating the diluted folds with peak areas of the intermediate compounds and GSH, respectively. Second, calibration factor of GSH (f_0) according to concentration (mmol/L) divided by peak area, was obtained by analysis of the 0.16-h reaction mixtures spiked with a known amount of GSH. Finally, concentration of the found intermediate compounds (C_i, mmol/L) in reaction mixtures was calculated by $C_i = (\rho / n) \times f_0 \times A_i$, where A_i was peak area of an intermediate compound in HPLC–MS analysis of the reaction mixtures, and n was equivalent numbers of cysteines in the molecule of the intermediate compound.

2.6. Analysis of volatile compounds from degradation of the intermediates

As in the case of the model reactions performed in Section 2.2, the intermediate compounds (L1, M2, M3, N4, and N5) (0.06 M, each) dissolved in phosphate buffer were heated at 140 °C for 2 h. Then the resulting solutions were analyzed by solid-phase microextraction (SPME) and gas chromatography–mass spectrometry (GC–MS) as follows.

Samples were pre-equilibrated at 50 °C for 10 min in a 15-mL SPME vial, and then extracted with the fiber (DVB/CAR/PDMS, 2 cm, 50/30 μm) (Supelco Inc., Bellefonte, PA) at the same temperature for 20 min in headspace mode. A 7890B gas chromatograph coupled with a 5975C mass spectrometer and a DB-Wax capillary column (30 m × 0.25 mm × 0.25 μm; Agilent Technologies, Santa Clara, CA) was used in analysis of the volatiles. The fiber was desorbed at 250 °C for 3 min in splitless mode. The GC oven was initially set at 35 °C for 2 min; raised to 60 °C at 2 °C/min, held for 2 min; and raised to 230 °C at 4 °C/min. Carrier gas was helium at 1.0 mL/min. Temperature of electron impact ion source (70 eV) was 230 °C. The mass detector was operated at 150 °C. Mass spectra were recorded over the range of m/z 33–450.

Identification of the volatile compounds was performed by search of NIST2015 mass database, comparison of the RIs (retention indices) relative to *n*-alkanes (C_5–C_{26}) with those documented in literature, and co-injection of available authentic chemicals. Amount of the volatile compounds was expressed as relative peak area (%), which was obtained by normalization of peak areas of the found compounds.

3. Results and discussion

3.1. HPLC–MS analysis

Reaction conditions were used according to our former investigation on the model systems of GSH and glucose with fat or oxidized fat (Zhao, Wang, Xie, Xiao, Cheng, et al., 2019). The resulting reaction mixtures were analyzed by HPLC–MS, while Fig. 1(a–g) showed total ion current (TIC) chromatograms of the 0.16-h reaction mixtures. As aforementioned, in the initial reaction of GSH, glucose, and aldehyde, both glucose and aldehyde can react with the GSH, forming non-volatile intermediate compounds. By comparison with the control reaction systems of GSH-glucose (GSH-Glu), GSH-hexanal (GSH-Hex), GSH-(*E*)-2-heptenal (GSH-Hept), or GSH-(*E*,*E*)-2,4-decadienal (GSH-Dec), it was seen that formation of G1, G2, G3, or G4 involved glucose, while that of L1, M1–M3, and N1-N6 involved hexanal, (*E*)-2-heptenal, and (*E*,*E*)-2,4-decadienal, respectively. The co-eluted peaks (e.g. G1 and M2 in Fig. 1(d)) were resolved by extracted ion chromatogram with $[M+H]^+$, based on the identified structures of the intermediate compounds shown in Figs. 2–5. In Fig. S1, the scheme for reaction of GSH, glucose, and the aldehydes to form the intermediate compounds is presented.

Concentrations of the intermediate compounds in the reaction mixtures of glucose-GSH-hexanal (Glu-GSH-Hex), glucose-GSH-(*E*)-2-heptenal (Glu-GSH-Hept), and glucose-GSH-(*E*,*E*)-2,4-decadienal (Glu-GSH-Dec) were determined according to Clark and Deed (2018), relative to the internal GSH, since authentic substances of most intermediate compounds were unavailable. As shown in Fig. 1(h–j), concentrations of all the intermediates first rose and then fell with reaction time. Regarding the glucose-derived intermediates (G1–G4), the maximum concentration occurred earliest for G4, then G3, and finally G2 or G1 for the reaction systems. According to chemical structures of the intermediates shown in Fig. 2, this peaking time order could be explained by that G4 was constructed from the starting materials of GSH and glucose, whereas G3 was from glucose and the cysteinylglycine (Cys-Gly) that was hydrolyzed from GSH or from a molecule with a GSH moiety later, and G1 and G2 were from Cys-Gly and a C3 or C4-fragment split from glucose or from a molecule with a glucose skeleton later. Following the same principle, as shown in Fig. 1(h–j), L1 (0.25 h)

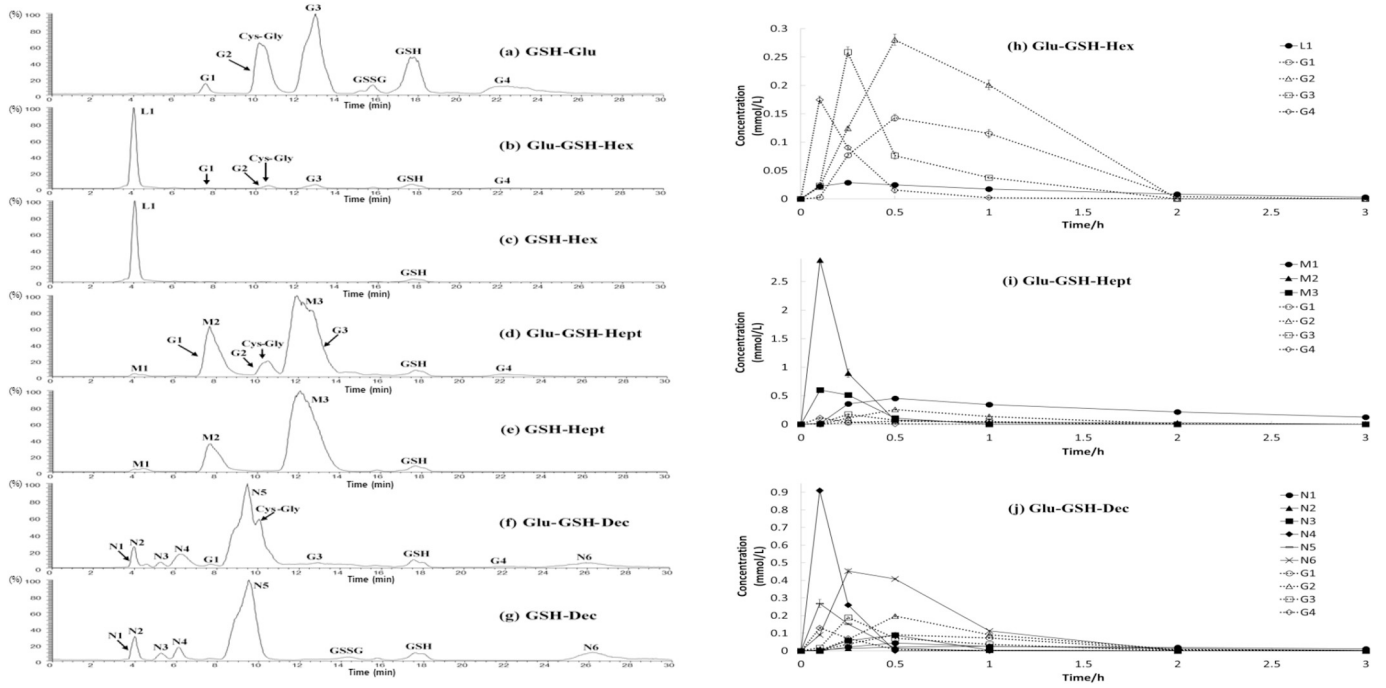

Fig. 1. (a–g). HPLC–MS total ion current chromatograms of 0.16-h reaction mixtures from both the target and the control reaction systems involving GSH, Glu, and/or aldehydes (hexanal, (*E*)-2-heptenal, or (*E*,*E*)-2,4-decadienal); and (h–j) trends of concentrations of the detected intermediate compounds with reaction time in the model systems of GSH, Glu, and the aldehydes (hexanal, (*E*)-2-heptenal, or (*E*,*E*)-2,4-decadienal).

peaked later than G4 in the Glu-GSH-Hex system. M2 or M3 was the earliest (0.16 h) to arrive at maximum concentration, followed by M1 (0.5 h) for the Glu-GSH-Hept system. For the Glu-GSH-Dec system, N4 or N5 was the earliest (0.16 h) to arrive at maximum concentration, followed by first N6 (0.25 h), then N1 and N3, and finally N2 (1 h). N2 had the latest peaking time because its formation involved not only Cys-Gly, but also hexanal that was later derived from the (*E*,*E*)-2,4-decadienal by retro-aldol reaction. On the other side, since GSH tended to hydrolyze the glutamyl, the earlier peaking intermediates with a GSH moiety (e.g., M2 and N4) exhibited a fast degradation, as shown in Fig. 1(h–j). However, the later peaking intermediates (e.g., M1 and N1) constructed with Cys-Gly decreased slowly along the timeline. Besides, with sharp degradation of the earlier peaking intermediates (e.g., M2 or N4), concentration of the later peaking intermediates (e.g., M1 or N1)

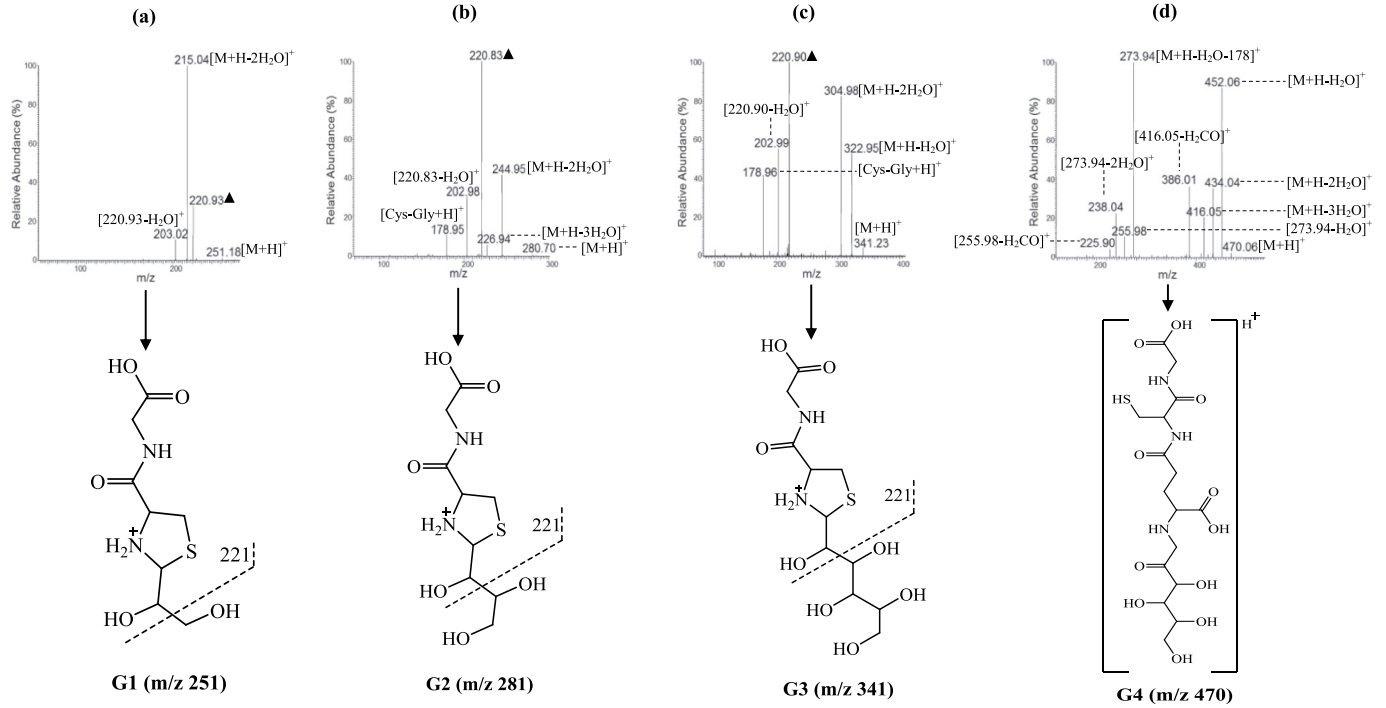

Fig. 2. MS/MS spectra and structural elucidation process of the detected glucose-derived intermediate compounds G1–G4. Note. ▲ Elucidation of the ion peak is shown in the molecule structure below.

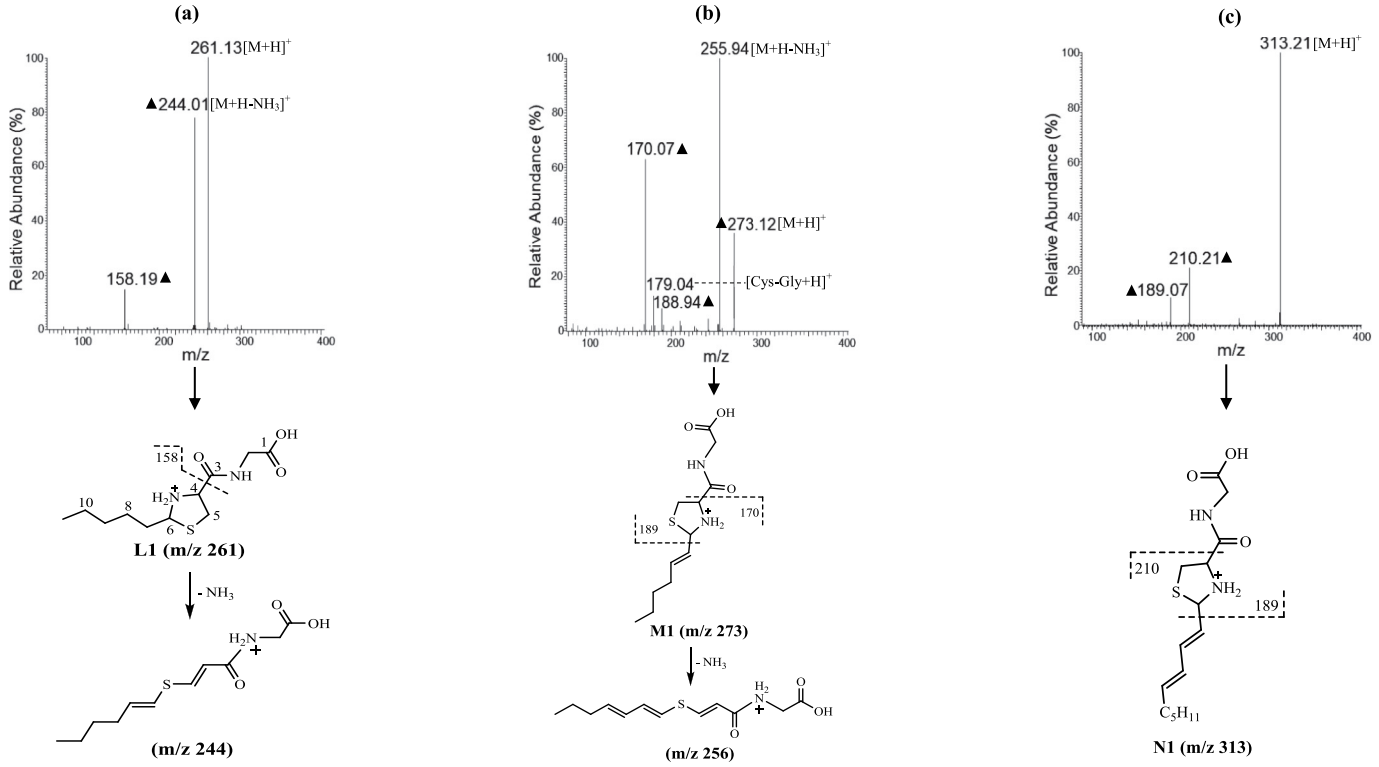

Fig. 3. MS/MS spectra and structural elucidation process of the aldehyde-derived intermediate compounds of thiazolidines (L1, M1, and N1) found in Glu-GSH-Hex, Glu-GSH-Hept, and Glu-GSH-Dec systems, respectively. Note. ▲ Elucidation of the ion peak is shown in the molecule structure below.

in the reaction solution was observed to increase, suggesting degradation of the former might help formation of the latter.

Formation of the intermediate compounds (L1, M1–M3, and N1–N6) with GSH or the hydrolyzed Cys-Gly indicated inhibition from the aldehydes (hexanal, (*E*)-2-heptenal, and (*E*,*E*)-2,4-decadienal) on the GSH-glucose reaction. In the Glu-GSH-Hex system, the glucose-derived intermediates G1–G4 had a concentration higher than the hexanal-derived intermediate L1. However, for the Glu-GSH-Hept or Glu-GSH-Dec system, the sum of concentrations of the aldehyde-derived intermediates (M1–M3, or N1–N6) was much above that of the glucose-derived intermediates (G1–G4). These suggested that (*E*)-2-heptenal and (*E*,*E*)-2,4-decadienal exhibited higher inhibition on the GSH-glucose reaction than hexanal, because of higher reactivity of the unsaturated aldehydes to react with GSH against glucose. Otherwise, according to our former research (Cao et al., 2017; Hou et al., 2017; Zhao, Wang, Xie, Xiao, Du, et al., 2019), except for the Amadori compound G4, the glucose-derived intermediates G1–G3 should also have inhibited the GSH-glucose reaction in development of sulfur-containing volatile flavors, because of their relatively stable thiazolidine structures. This was evidenced from their tardy degradation with time, as obviously seen from Fig. 1(h).

3.2. Structure identification by MS

MS spectra corresponding to the above HPLC–MS analysis and structural elucidation process were shown in Figs. 2–5. According to Fig. 2, G1, G2, and G3 were identified to be thiazolidine derivatives formed from reaction of Cys-Gly with a fragment of glucose (G1, G2) or glucose itself (G3). G4 was the Amadori compound formed from reaction of glucose and GSH. Among them, the chemical structures of G3 and G4 had been found from a Glu-GSH system by Jerić and Horvat (2009), but no report exists for those of G1 and G2. In Fig. 2, the ion *m/z* 221 due to scission in the carbohydrate chain of the $[M+H]^+$ ion all had a good abundance for G1, G2, and G3, indicating vulnerability of the carbohydrate chain in collision-induced dissociation (CID) during MS/MS analysis. Besides, the ions *m/z* 215 for G1, *m/z* 245 for G2, and *m/z* 323 and 305 for G3 with loss of one or two molecules of water from the carbohydrate moiety of the respective $[M+H]^+$ were revealed with a strong peak. The ion *m/z* 203 due to loss of one molecule of water from the carbohydrate moiety of the aforementioned *m/z* 221 ion also exhibited a considerable abundance in G1, G2, and G3. Otherwise, the ion of Cys-Gly (178) for G2 or G3 and the ion *m/z* 227 with loss of three molecules of water from the $[M+H]^+$ ion for G2 were also detected. With regards to the Amadori compound G4, similarly, the *m/z* 452, 434, and 416 ions were attributed to consecutive loss of water from the carbohydrate moiety of the $[M+H]^+$ (470) (Linetsky, Shipova, Legrand, & Argirov, 2005). The relatively strong peak of *m/z* 386 represented a stable immonium ion with removal of three molecules of water and one molecule of formaldehyde from the carbohydrate moiety of the $[M+H]^+$ (Jerić & Horvat, 2009; Jerić, Versluis, Horvat, & Heck, 2002). The strong peak of *m/z* 274 ion might be acquired by loss of Cys-Gly (178) as well as one molecule of water from the $[M+H]^+$ (470) (Jerić & Horvat, 2009). The ion *m/z* 274 through first loss of one molecule of water and then another, could lead to the *m/z* 256 ion and the *m/z* 238 ion, respectively. The *m/z* 256 ion with cleavage of one molecule of formaldehyde from the carbohydrate chain could lead to the *m/z* 226 ion.

As shown in Fig. 3, L1, M1, and N1 were thiazolidine derivatives generated by hexanal, (*E*)-2-heptenal, or (*E*,*E*)-2,4-decadienal reacted with both the groups of sulfhydryl and amino of Cys-Gly. Since (*E*,*E*)-2,4-decadienal could transform into hexanal via retro-aldol reaction, the intermediate compound (named N2 herein) with structure of L1 was also detected in the reaction systems involving (*E*,*E*)-2,4-decadienal. Moreover, as shown in Fig. 4, M2 and N4 had the chemical structures of hemiacetals formed by sulfhydryl of the GSH attacked by the carbonyl of (*E*)-2-heptenal and (*E*,*E*)-2,4-decadienal, respectively. As shown in Fig. 5, M3, N3, N5, and N6 were complex thiazolidine derivatives formed from (*E*)-2-heptenal or (*E*,*E*)-2,4-decadienal reacted with one

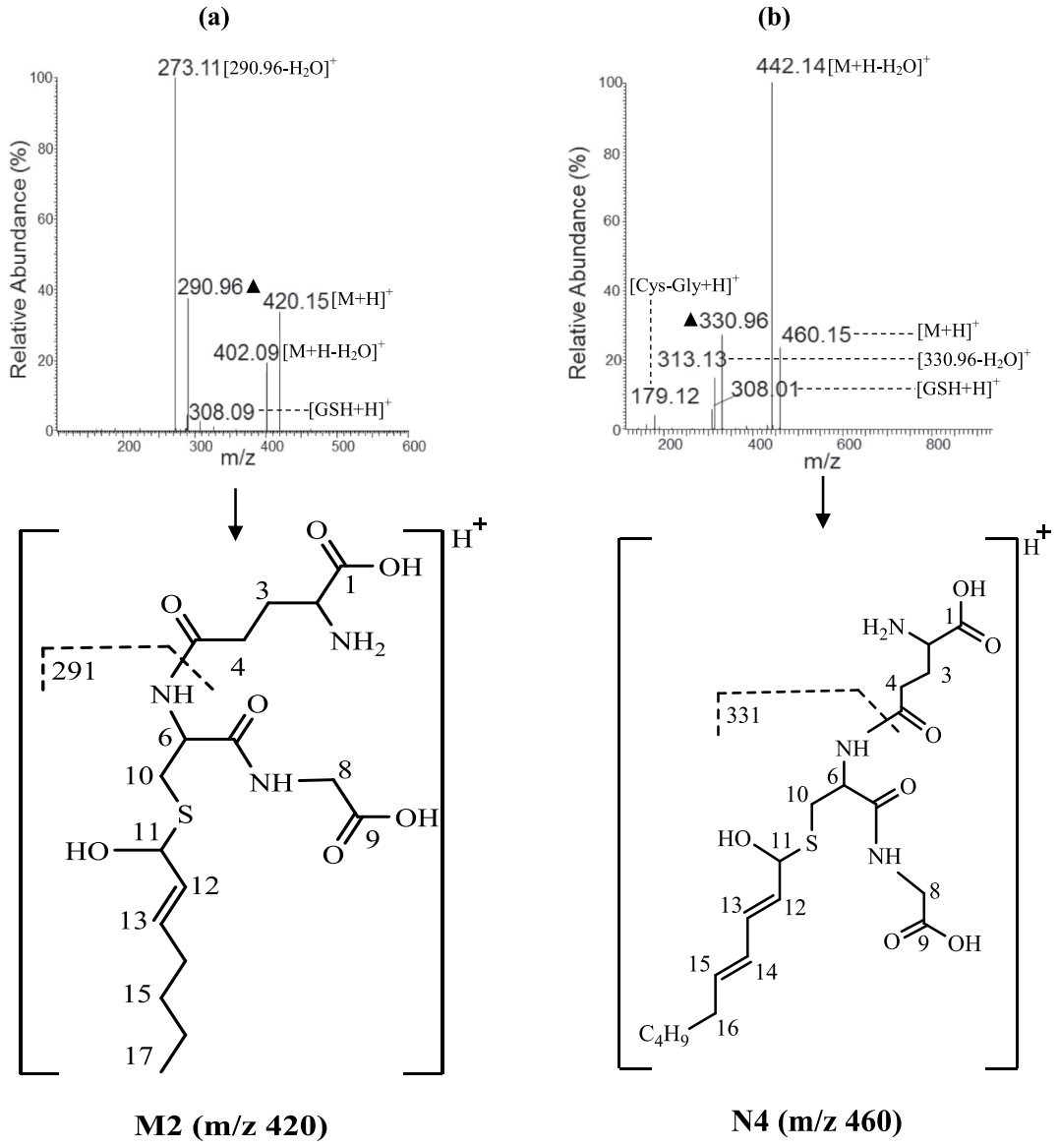

Fig. 4. MS/MS spectra and structural elucidation process for the aldehyde-derived intermediate compounds of hemiacetals (M2 and N4) found from Glu-GSH-Hept system and Glu-GSH-Dec system, respectively. Note. ▲ Elucidation of the ion peak is shown in the molecule structure below.

molecule of glutathione and one molecule of Cys-Gly (M3 and N5), two molecules of Cys-Gly (N3), or one molecule of glutathione and two molecules of Cys-Gly (N6). Notably, formation of L1, M1, and N1 involved nucleophilic addition of both the sulfhydryl and the amino groups towards the aldehyde group, and formation of M2 and N4 involved nucleophilic addition of the sulfhydryl towards the aldehyde group; all of which created a chiral center and led to a mixture of two diastereoisomers (Block et al., 2018; Fernandez et al., 2001). In addition, formation of the complex thiazolidine derivatives M3, N3, N5, and N6 not only involved the aforementioned classical carbonyl addition, but also the 1,4-conjugate addition (Michael addition) of sulfhydryl towards the conjugated carbon–carbon double bond of the *α,β*-unsaturated aldehydes, which created another chiral center and led to the mixture with a doubled number of diastereoisomers (Clark & Deed, 2018).

Different from G1, G2, and G3, L1, M1, and N1 all had a strong peak for the $[M+H]^+$ ion (e.g., *m/z* 261 for L1) (see Fig. 3), due to presence of a hydrocarbon chain in these thiazolidine derivatives, instead of that of a carbohydrate chain. Besides, another strong peak of *m/z* 244 for L1 and of *m/z* 256 for M1 with elimination of NH_3 from the $[M+H]^+$ ions of L1 and M1, respectively, were detected. The resulted high abundance with the *m/z* 244 and 256 ions might be due to the presence of a relatively stable structure of conjugated amide in the two ions. Moreover, the ions *m/z* 158 for L1, *m/z* 170 for M1, and *m/z* 210 for N1 could all be acquired by cleavage of the amide chain from the respective $[M+H]^+$ ion. The ion *m/z* 189 for M1 or N1 could be acquired by removal of the alkene chain from the respective $[M+H]^+$ ion.

As shown in Fig. 4, either M2 or N4 was characterized by a strong peak of $[M+H-H_2O]^+$ because of the hydroxyl group of hemiacetal. However, the weak peak of $[M+H-H_2O]^+$ for M3, N5, and N6 (shown in Fig. 5) was ascribed to the presence of the GSH moiety, since GSH also had such a weak peak of $[M+H-H_2O]^+$ during MS detection (data not shown). Overall, the hemiacetals (M2 and N4) and the complex thiazolidines (M3, N3, N5, and N6) mainly had the following types of scission in MS/MS analysis: cleavage of the glutamyl (e.g., *m/z* 291 for M2, 331 for N4, 451 for M3, 491 for N5, and 669 for N6), reversible loss of the Cys-Gly (e.g., *m/z* 313 for N3 and *m/z* 620 for N6), reversible loss of the GSH (e.g., *m/z* 273 for M3, 313 for N5, and 491 for N6), or reversible loss of both the Cys-Gly and the GSH (e.g., *m/z* 313 for N6). Consequently, in addition to the ions of GSH (*m/z* 308) and Cys-Gly (*m/*

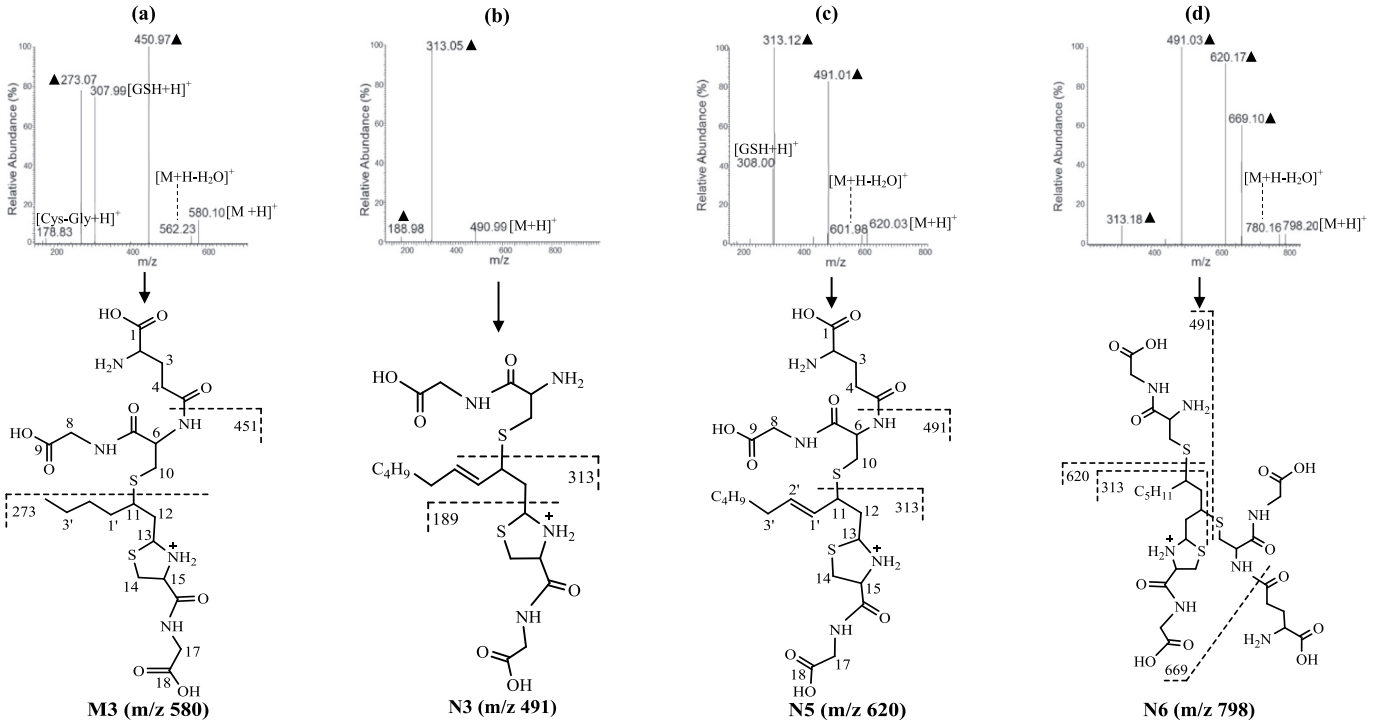

Fig. 5. MS/MS spectra and structural elucidation process of the aldehyde-derived intermediate compounds of complex thiazolidines (M3, N3, N5, and N6) found from Glu-GSH-Hept system and Glu-GSH-Dec system, respectively. Note. ▲ Elucidation of the ion peak is shown in the molecule structure below.

z 179), the fragment ions with a structure of M1 (*m/z* 273) or N1 (*m/z* 313) were also detected from the hemiacetals (M2 and N4) and the complex thiazolidines (M3, N3, N5, and N6). Regarding the hemiacetals (M2 and N4), possibly the ions *m/z* 291 for M2 and *m/z* 331 for N4 (see Fig. 4) with cleavage of the glutamyl from the $[M+H]^+$ ions went through such a reaction, i.e., the hemiacetal carbon was attacked by the amino group, followed by elimination of water, resulting in ions with the structures of M1 (*m/z* 273) and N1 (*m/z* 313), respectively.

3.3. Structure identification by NMR

Preparation of the aldehyde-derived intermediates was performed by separation of GSH-aldehyde reaction mixtures, in order to further identify structures of the found intermediates by NMR and to subsequently investigate roles of the intermediate compounds in development of volatile flavors. As a result, the substances of L1, M2, M3, N4, and N5 with identities as those in the above HPLC–MS analysis were obtained with a high purity by HPLC analysis using the universal detection of ELSD.

The processed NMR data were presented in Section 2.3, while the NMR spectra are shown in Figs. S2–S6. Comparing with those of the original aldehydes (hexanal, (*E*)-2-heptenal, and (*E*,*E*)-2,4-decadienal) and those of the GSH, ^{1}H NMR and ^{13}C NMR data of the prepared intermediate compounds revealed most information from the skeletons of the original aldehydes or the GSH, which were not discussed in the following. Besides, there were signals of trace impurities or environmental contaminants found in the NMR spectra. However, obvious signals of the aldehyde group or the sulfhydryl group were not detected for the intermediate compounds. With regards to L1, chemical shifts (ppm) of δ_C 64.91/δ_H 4.64 (C-6), δ_C 35.37/δ_H 3.16 (C-5), and δ_C 69.84/δ_H 3.74 (C-4) corresponding to the thiazolidine ring were consistent with the literature (Corbi et al., 2008; Fernandez et al., 2001; Starkenmann, 2003); likewise for M3 and N5. Moreover, for M3, both ^{1}H NMR and ^{13}C NMR signals did not reveal any information of an olefinic bond, whereas chemical shifts (ppm) of δ_C 44.45/δ_H 2.63 (C-11) and δ_C 38.68/δ_H 2.03 (C-12) indicated the saturated carbons after Michael addition reaction of the sulfhydryl group to the olefinic bond of (*E*)-2-heptenal (Starkenmann, 2003). For N5, the chemical shifts (ppm) of δ_C 128.81/δ_H 5.57 (C-1′) and δ_C 135.67/δ_H 5.47 (C-2′) corresponded to an olefinic bond. The chemical shifts (ppm) of δ_C 52.48/δ_H 3.16 (C-11) revealed that the sulfhydryl group was added at the unsaturated carbon at the *β*-position to the aldehyde group of (*E*,*E*)-2,4-decadienal, while those of δ_C 39.77/δ_H 2.03 (C-12) corresponded to the saturated carbon with addition of hydrogen to the *α*-position unsaturated carbon of the olefinic bond (Starkenmann, 2003).

Regarding M2, chemical shifts (ppm) of δ_C 125.82 (C-12) and 129.14 (C-13) indicated the presence of an olefinic bond. Regarding N4, chemical shifts (ppm) of δ_C 128.75/δ_H 5.53 (C-12), δ_C 128.63/δ_H 6.18 (C-13), δ_C 128.59/δ_H 5.63 (C-14), and δ_C 133.98/δ_H 5.33 (C-15) indicated the presence of a conjugated carbon–carbon double bond (Zhao et al., 2018). Due to disappearance of the aldehyde group, the above values of olefinic bond chemical shifts for M2 and N4 were obviously smaller than those of the original (*E*)-2-heptenal or (*E*,*E*)-2,4-decadienal (data not shown). Moreover, the assignment of δ_C 89.26/δ_H 5.04 ppm (C-11) for M2 and δ_C 78.96/δ_H 5.18 ppm (C-11) for N4, corresponding to a hetero hemiacetal with S atom and O atom, agreed with the literature (Block et al., 2018). Otherwise, it seemed that tautomerization might occur for the hemiacetals in D_2O. For M2 (see Fig. S5), signals (ppm) of δ_C 206.38 (C-12′), δ_C 57.52 (C-6′), δ_C 39.51 (C-13′), δ_C 38.59/δ_H 3.17 (C-11′), δ_C 28.11/δ_H 3.02 (C-10′), and δ_C 24.66/δ_H 1.52 (C-14′) might be ascribed to the tautomer with a ketone group from the hemiacetal. For N4 (see Fig. S6), signals (ppm) of δ_C 149.08/δ_H 6.79 (C-13′), δ_C 122.34 (C-12′), δ_C 58.30/δ_H 4.23 (C-6′), δ_C 35.40 (C-14′), δ_C 33.36/δ_H 3.19 (C-10′), and δ_C 28.00/δ_H 1.50 (C-15′) might be ascribed to the structure of tautomer (i) by transfer of hydrogen proton of the hydroxy group of the hemiacetal from C-11 to C-15. Also for N4 (see Fig. S6), signals (ppm) of δ_C 81.82 (C-12″), δ_C 64.68 (C-6″), δ_C 25.30 (C-13″), and δ_H 3.19 (C-10″) might be ascribed to the structure of tautomer (ii), due to transfer of hydrogen proton of the hydroxy group of the hemiacetal from C-11 to C-13. Anyway, the aforementioned tautomerization needs to be further proved, since some NMR signals of the tautomers were not discerned, as their peaks could be overlapped with

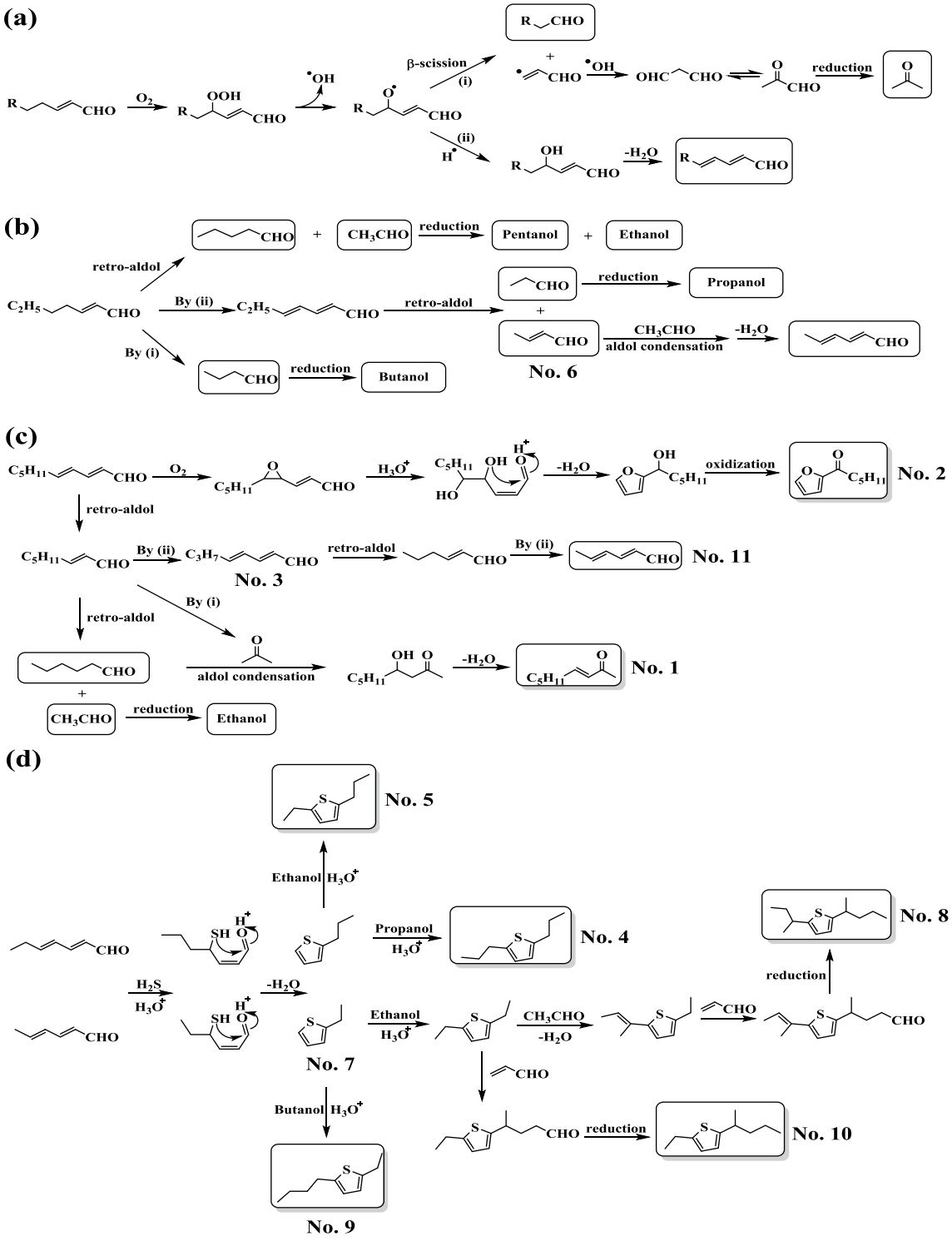

Fig. 6. Possible pathways for (a) formation of (*E*,*E*)-2,4-dienals and acetone by radical oxidation of the (*E*)-2-alkenals. (b) formation of some new aliphatic compounds from (*E*)-2-heptenal via retro-aldol condensation, oxidation, reduction, etc. (c) formation of some new aliphatic compounds in particular (*E*)-3-nonen-2-one (No. 1) and 2-hexanoylfuran (No. 2) from (*E*,*E*)-2,4-decadienal via retro-aldol condensation, oxidation, reduction, etc. (d) formation of the dialkyl thiophenes, namely, 2,5-dipropylthiophene (No. 4), 2-ethyl-5-propylthiophene (No. 5), 2-*sec*-butyl-5-(1-methylbutyl)thiophene (No. 8), 2-butyl-5-ethylthiophene (No. 9), and 2-ethyl-5-(1-methylbutyl)thiophene (No. 10) by H_2S reacting with the resulting aliphatic products, especially the new aldehydes from (*E*)-2-heptenal or (*E*,*E*)-2,4-decadienal, as shown in (a–c).

those of the hemiacetals.

Above all, according to the empirically estimated values, chemical shifts (ppm) of the allylic carbons by ^{13}C NMR, i.e., 89.26 (C-11) and 34.12 (C-14) for M2, 78.96 (C-11) and 38.69 (C-16) for N4, and 52.48 (C-11) and 36.42 (C-3′) for N5 were consistent with those of the (*E*)-configuration of a di-substituted carbon–carbon double bond. Therefore, probably M2, N4, and N5 kept the (*E*)-configuration as the original used (*E*)-2-heptenal or (*E*,*E*)-2,4-decadienal.

3.4. Volatile flavor compounds formed from degradation of the intermediate compounds

Solutions of the prepared intermediate compounds (L1, M2, M3, N4, and N5) were heated as the model reaction systems for 2 h, as they were observed able to be completely degraded in 2 h, as shown in Fig. 1(h–j). In fact, GC–MS detected more than a hundred chromatographic peaks in each heated solution; it was found that identifications between M2 and M3 solutions or between N4 and N5 solutions were almost the same, as shown in Table S1. The original aldehydes of hexanal, (*E*)-2-heptenal, and (*E*,*E*)-2,4-decadienal or the (*E*)-2-heptenoic acid oxidized from (*E*)-2-heptenal were revealed with the highest level in the respective solution. This indicated that during heating, these intermediate compounds were reversibly reacted to release the original reactants. Fig. 6 shows possible formation pathways of some identified compounds. Overall, the released aldehydes (hexanal, (*E*)-2-heptenal or (*E*,*E*)-2,4-decadienal) undertook retro-aldol or aldol condensation, oxidation, cyclization, and reduction, etc., leading to the various new aldehydes, ketones, alcohols, furans, etc., listed in Table S1. For example, aldol condensation of hexanal could account for the major compound 2-butyl-(*E*)-2-octenal found in L1 solution. Regarding the high level of 3-nonen-2-one in N4 and N5 solutions, it was probably formed from aldol condensation of hexanal and acetone, as shown in Fig. 6(c) for compound No. 1. Among them, hexanal was formed from (*E*,*E*)-2,4-decadienal by retro-aldol reactions, while acetone was from (*E*,*E*)-2,4-decadienal through a series of reactions including retro-aldol, oxidation, *β*-scission, tautomerization, and reduction, as shown in Fig. 6(c) and (a). Moreover, 2-pentyl-2-cyclopenten-1-one was formed from cyclization of (*E*,*E*)-2,4-decadienal (Adams, Kitrytė, Venskutonis, & De Kimpe, 2011). The high level of 2-hexanoylfuran (No. 2) could be formed from (*E*,*E*)-2,4-decadienal through alkene epoxidation and ring opening, cyclization, loss of water, and oxidization. The identified 2-propylfuran, 2-butylfuran, and 2-pentylpyran/2-hexylfuran from M2, M3, N4, or N5 solution could result from cyclization of (*E*,*E*)-2,4-heptadienal, (*E*,*E*)-2,4-octadienal, and (*E*,*E*)-2,4-decadienal, in turn (Adams, Bouckaert, Van Lancker, De Meulenaer, & De Kimpe, 2011; Mottram, 1998). Among them, (*E*,*E*)-2,4-heptadienal and (*E*,*E*)-2,4-octadienal (No. 3, see Fig. 6(c)) were oxidized from (*E*)-2-heptenal and (*E*)-2-octenal, respectively, according to the proposed Way (ii) reactions in Fig. 6(a); while the (*E*)-2-octenal could be formed from (*E*,*E*)-2,4-decadienal via retro-aldol reaction, as shown in Fig. 6(c).

Like our previous findings from GSH-glucose with fat or oxidized fat model reaction systems (Zhao, Wang, Xie, Xiao, Cheng, et al., 2019), as shown in Table S1, several alkyl sulfur- or nitrogen-containing compounds (e.g., 2-hexylthiophene and 2-ethylpyridine) were found. Worth mentioning, these listed alkyl compounds were also detected in the corresponding model systems of GSH and aldehyde (hexanal, (*E*)-2-heptenal or (*E*,*E*)-2,4-decadienal) with or without glucose (data not shown). This indicated that these model reaction systems passed in the same way via these intermediates to form the volatile flavors. During heating, thermal degradation of GSH in particular the Strecker degradation of cysteine from GSH induced by the lipid degradation products (e.g. (*E*)-2-heptenal) can release H_2S and NH_3 (Gallardo et al., 2008; Hidalgo & Zamora, 2016). The identified 1-hexanethiol in L1 solution could be formed from reaction of 1-hexanol and H_2S, while reduction of hexanal could lead to the 1-hexanol (Zhao, Wang, Xie, Xiao, Cheng, et al., 2019). (*E*,*E*)-2,4-Heptadienal and (*E*,*E*)-2,4-decadienal via epoxidation, addition of H_2S, and oxidization could form the 1-(2-thienyl)-1-propanone in M2 and M3 solutions and the 1-(2-thienyl)-1-hexanone in N4 and N5 solutions, respectively (Zhao, Wang, Xie, Xiao, Cheng, et al., 2019). 1-(2-Pyridinyl)-1-pentanone could be generated in the same way as 1-(2-thienyl)-1-hexanone, with NH_3 involved instead of H_2S. (*E*,*E*)-2,4-Heptadienal, (*E*,*E*)-2,4-octadienal, and (*E*,*E*)-2,4-decadienal reacting with H_2S could form the 2-propylthiophene, 2-butylthiophene, and 2-pentylthiopyran/2-hexylthiophene, in turn (Elmore & Mottram, 2000). But in the presence of NH_3, amino acids, or the GSH, the aforementioned reaction of (*E*,*E*)-2,4-heptadienal and (*E*,*E*)-2,4-decadienal could lead to 2-ethylpyridine and 2-pentylpyridine, respectively (Mottram, 1998; Zhang & Ho, 1989).

Particularly, six dialkylthiophenes (see Table S1) were found at a high or considerable level, namely, 2,5-dipropylthiophene, 2-ethyl-5-propylthiophene, 2-butyl-5-propylthiophene, 2-butyl-5-ethylthiophene, and 2-*sec*-butyl-5-(1-methylbutyl)thiophene in M2 or M3 solution, and 2-ethyl-5-(1-methylbutyl)thiophene in N4 or N5 solution. As shown in Fig. 6(d), regarding the dialkylthiophenes found in M2 or M3 solution, possibly, 1-propanol and ethanol reacting with the aforementioned 2-propylthiophene via electrophilic substitution reaction formed 2,5-dipropylthiophene (No. 4) and 2-ethyl-5-propylthiophene (No. 5), respectively. 2-Butenal (No. 6, in Fig. 6(b)) reacting with acetaldehyde via aldol condensation followed by elimination of water formed (*E*,*E*)-2,4-hexadienal, which subsequently reacted with H_2S to form 2-ethylthiophene (No. 7, in Fig. 6(d)). The 2-ethylthiophene reacting with ethanol, acetaldehyde, and acrolein followed by reduction led to 2-*sec*-butyl-5-(1-methylbutyl)thiophene (No. 8). 1-Butanol reacting with 2-ethylthiophene via electrophilic substitution reaction formed 2-butyl-5-ethylthiophene (No. 9). Regarding the 2-ethyl-5-(1-methylbutyl)thiophene (No. 10) in N4 or N5 solution, as shown in Fig. 6(d), it was proposed that first 2-ethylthiophene was formed, then electrophilic substitution by ethanol, addition of acrolein, and reduction occurred. However, herein, the (*E*,*E*)-2,4-hexadienal in formation of 2-ethylthiophene might be originated from the (*E*,*E*)-2,4-decadienal by two-times retro-aldol reactions and two-times Way (ii) reactions, as shown in Fig. 6(c) for compound No. 11, while the Way (ii) reactions were shown in Fig. 6(a).

4. Conclusions

Initial reaction intermediate compounds were identified from the model systems composed of glucose, GSH, and hexanal, (*E*)-2-heptenal, or (*E*,*E*)-2,4-decadienal by HPLC-MS as well as NMR. Except for the Amadori compounds and hemiacetals, all the others had relatively stable structures of thiazolidines. In addition, degradation of the intermediates with a GSH moiety by removal of the glutamyl contributed to formation of those relatively stable thiazolidines. The unsaturated aldehydes (*E*)-2-heptenal and (*E*,*E*)-2,4-decadienal exhibited much stronger reactivity against glucose to react with GSH, which resulted in the sum of concentrations of intermediate compounds being over more than the glucose-derived intermediates or above the glucose-derived intermediates. During heating, the aldehyde-derived intermediates mainly released the original aldehydes, which induced formation of various new aliphatic products through retro-aldol or aldol condensation, oxidation, cyclization, and reduction, etc. Both the original aldehydes and the new aliphatic compounds could react with H_2S or NH_3 to form alkyl sulfur-containing or nitrogen-containing compounds. Particularly, formation pathways of 3-nonen-2-one, 2-hexanoylfuran, and six 2,5-dialkylthiophenes, found at high or considerable levels in the heated solutions, were proposed for the first time. The work is helpful for gaining insight into formation of meat flavor in processing of meat or meat-like foods.

Supplementary data to this article can be found online at https://doi.org/10.1016/j.foodchem.2019.125482.

Declaration of competing interest

The authors declare that they have no known competing financial interests or personal relationships that could have appeared to influence the work reported in this paper.

Acknowledgements

The present work was supported by the National Natural Science Foundation of China (31671895), Beijing Municipal Natural Science

Foundation (6172004), and National Key Research and Development Program of China (2017YFD0400106).

Compliance with ethical standards

This article does not contain any studies with human participants or animals performed by any of the authors.

References

Adams, A., Bouckaert, C., Van Lancker, F., De Meulenaer, B., & De Kimpe, N. (2011). Amino acid catalysis of 2-alkylfuran formation from lipid oxidation-derived *α,β*-unsaturated aldehydes. Journal of Agricultural and Food Chemistry, 59(20), 11058–11062. doi:https://doi.org/10.1021/jf202448v.

Adams, A., Kitrytė, V., Venskutonis, R., & De Kimpe, N. (2011). Model studies on the pattern of volatiles generated in mixtures of amino acids, lipid-oxidation-derived aldehydes, and glucose. *Journal of Agricultural and Food Chemistry, 59*(4), 1449–1456. https://doi.org/10.1021/jf104091p.

Block, E., Dethier, B., Bechand, B., Cotelesage, J. J. H., George, G. N., Goto, K., ... Vogt, L. (2018). Ajothiolanes: 3,4-Dimethylthiolane natural products from garlic (*Allium sativum*). *Journal of Agricultural and Food Chemistry, 66*(39), 10193–10204. https://doi.org/10.1021/acs.jafc.8b03638.

Cao, C., Xie, J., Hou, L., Zhao, J., Chen, F., Xiao, Q., ... Fan, M. (2017). Effect of glycine on reaction of cysteine-xylose: Insights on initial Maillard stage intermediates to develop meat flavor. *Food Research International, 99*, 444–453. https://doi.org/10.1016/j.foodres.2017.06.012.

Clark, A. C., & Deed, R. C. (2018). The chemical reaction of glutathione and *trans*-2-hexenal in grape juice media to form wine aroma precursors: The impact of pH, temperature, and sulfur dioxide. *Journal of Agricultural and Food Chemistry, 66*(5), 1214–1221. https://doi.org/10.1021/acs.jafc.7b04991.

Corbi, P. P., Andrade, F. C., Massabni, A. C., Heinrich, T. A., Souza, P. P. C., & Costa-Neto, C. M. (2008). Lithium thiazolidine-4-carboxylate: Synthesis, spectroscopic characterization and preliminary *in vitro* cytotoxic studies in human HeLa cells. *Spectrochimica Acta Part A, 71*(3), 929–931. https://doi.org/10.1016/j.saa.2008.02.013.

El-massry, K., Farouk, A., & El-Ghorab, A. (2003). Volatile constituents of glutathione-ribose model system and its antioxidant activity. *Amino Acids, 24*(1–2), 171–177. https://doi.org/10.1007/s00726-002-0318-4.

Elmore, J. S., Campo, M. M., Enser, M., & Mottram, D. S. (2002). Effect of lipid composition on meat-like model systems containing cysteine, ribose, and polyunsaturated fatty acids. *Journal of Agricultural and Food Chemistry, 50*(5), 1126–1132. https://doi.org/10.1021/jf0108718.

Elmore, J. S., & Mottram, D. S. (2000). Formation of 2-alkyl-(2*H*)-thiapyrans and 2-alkylthiophenes in cooked beef and lamb. *Journal of Agricultural and Food Chemistry, 48*(6), 2420–2424. https://doi.org/10.1021/jf000124v.

Farmer, L. J., & Mottram, D. S. (1990). Interaction of lipid in the Maillard reaction between cysteine and ribose: The effect of a triglyceride and three phospholipids on the volatile products. *Journal of the Science of Food and Agriculture, 53*(4), 505–525. https://doi.org/10.1002/jsfa.2740530409.

Fernandez, X., Duñach, E., Fellous, R., Lizzani-Cuvelier, L., Loiseau, M., Dompe, V., ... Schippa, C. (2001). Identification of thiazolidines in guava: Stereochemical studies. *Flavour and Fragrance Journal, 16*(4), 274–280. https://doi.org/10.1002/ffj.996.

Gallardo, E., de Schutter, D. P., Zamora, R., Derdelinckx, G., Delvaux, F. R., & Hidalgo, F. J. (2008). Influence of lipids in the generation of phenylacetaldehyde in wort-related model systems. *Journal of Agricultural and Food Chemistry, 56*(9), 3155–3159. https://doi.org/10.1021/jf800094k.

Hidalgo, F. J., & Zamora, R. (2016). Amino acid degradations produced by lipid oxidation products. *Critical Reviews in Food Science and Nutrition, 56*(8), 1242–1252. https://doi.org/10.1080/10408398.2012.761173.

Hou, L., Xie, J., Zhao, J., Zhao, M., Fan, M., Xiao, Q., ... Chen, F. (2017). Roles of different initial Maillard intermediates and pathways in meat flavor formation for cysteine-xylose-glycine model reaction systems. *Food Chemistry, 232*, 135–144. https://doi.org/10.1016/j.foodchem.2017.03.133.

Jerić, I., & Horvat, Š. (2009). Screening for glucose-triggered modifications of glutathione. *Journal of Peptide Science, 15*(8), 540–547. https://doi.org/10.1002/psc.1159.

Jerić, I., Versluis, C., Horvat, Š., & Heck, A. J. R. (2002). Tracing glycoprotein structures: Electron ionization tandem mass spectrometric analysis of sugar-peptide adducts. *Journal of Mass Spectrometry, 37*(8), 803–811. https://doi.org/10.1002/jms.337.

Lee, S. M., Jo, Y.-J., & Kim, Y.-S. (2010). Investigation of the aroma-active compounds formed in the Maillard reaction between glutathione and reducing sugars. *Journal of Agricultural and Food Chemistry, 58*(5), 3116–3124. https://doi.org/10.1021/jf9043327.

Linetsky, M. D., Shipova, E. V., Legrand, R. D., & Argirov, O. O. (2005). Glucose-derived Amadori compounds of glutathione. *Biochimica et Biophysica Acta, 1724*(1–2), 181–193. https://doi.org/10.1016/j.bbagen.2005.04.003.

Liu, P., Zhang, X., Huang, M., Song, S., & Nsor-Atindana, J. (2012). Formation mechanism of cross-linking Maillard compounds in peptide-xylose systems. *Journal of Peptide Science, 18*(10), 626–634. https://doi.org/10.1002/psc.2443.

Mottram, D. S. (1998). Flavour formation in meat and meat products: A review. *Food Chemistry, 62*(4), 415–424. https://doi.org/10.1016/S0308-8146(98)00076-4.

Pan, K.-L., Huang, W.-J., Hsu, M.-H., Lee, H.-L., Liu, H.-J., Cheng, C.-W., Tsai, M.-H., Shen, M.-Y., & Lin, P. (2014). Identification of *trans*,*trans*-2,4-decadienal metabolites in mouse and human cells using liquid chromatography-mass spectrometry. Chemical Research in Toxicology, 27(10), 1707–1719. doi:https://doi.org/10.1021/tx500199b.

Schumacher, F., Neuber, C., Finke, H., Nieschalke, K., Baesler, J., Gulbins, E., & Kleuser, B. (2017). The sphingosine 1-phosphate breakdown product, (2*E*)-hexadecenal, forms protein adducts and glutathione conjugates in vitro. *Journal of Lipid Research, 58*(8), 1648–1660. https://doi.org/10.1194/jlr.M076562.

Starkenmann, C. (2003). Analysis of a model reaction system containing cysteine and (*E*)-2-methyl-2-butenal, (*E*)-2-hexenal, or mesityl oxide. *Journal of Agricultural and Food Chemistry, 51*(24), 7146–7155. https://doi.org/10.1021/jf0304268.

Thibon, C., Böcker, C., Shinkaruk, S., Moine, V., Darriet, P., & Dubourdieu, D. (2016). Identification of *S*-3-(hexanal)-glutathione and its bisulfite adduct in grape juice from *Vitis vinifera* L. cv. Sauvignon blanc as new potential precursors of 3SH. *Food Chemistry, 199*, 711–719. https://doi.org/10.1016/j.foodchem.2015.12.069.

Yang, Z., Xie, J., Zhang, L., Du, R., Cao, C., Wang, M., ... Sun, B. (2015). Aromatic effect of fat and oxidized fat on a meat-like model reaction system of cysteine and glucose. *Flavour and Fragrance Journal, 30*(4), 320–329. https://doi.org/10.1002/ffj.3248.

Zhang, Y., & Ho, C.-T. (1989). Volatile compounds formed from thermal interaction of 2,4-decadienal with cysteine and glutathione. *Journal of Agricultural and Food Chemistry, 37*(4), 1016–1020. https://doi.org/10.1021/jf00088a044.

Zhao, J., Wang, T., Xie, J., Xiao, Q., Cheng, J., Chen, F., ... Sun, B. (2019a). Formation mechanism of aroma compounds in a glutathione-glucose reaction with fat or oxidized fat. *Food Chemistry, 270*(1), 436–444. https://doi.org/10.1016/j.foodchem.2018.07.106.

Zhao, J., Wang, T., Xie, J., Xiao, Q., Du, W., Wang, Y., ... Wang, S. (2019b). Meat flavor generation from different composition patterns of initial Maillard stage intermediates formed in heated cysteine-xylose-glycine reaction systems. *Food Chemistry, 274*, 79–88. https://doi.org/10.1016/j.foodchem.2018.08.096.

Zhao, J.-Y., Ding, J.-H., Li, Z.-H., Feng, T., Zhang, H.-B., & Liu, J.-K. (2018). Two new polyols from cultures of the fungus *Daedaleopsis tricolor*. *Natural Product Research, 32*(9), 1076–1079. https://doi.org/10.1080/14786419.2017.1380013.

Zhou, R., Grant, J., Goldberg, E. M., Ryland, D., & Aliani, M. (2018). Investigation of low molecular weight peptides (< 1 kDa) in chicken meat and their contribution to meat flavor formation. *Journal of the Science of Food and Agriculture, 99*(4), 1728–1739. https://doi.org/10.1002/jsfa.9362.